

Article

Photocatalytic Performance and Kinetic Studies of a Wood Surface Loaded with Bi₂O₃-Doped Silicon–Titanium Composite Film

Zhigao Liu ¹ , Jinchi Xu ¹, Si Cheng ², Zhiyong Qin ¹ and Yunlin Fu ^{1,2,*}¹ College of Resources, Environment and Materials, Guangxi University, Nanning 530004, China² College of Forestry, Guangxi University, Nanning 530004, China

* Correspondence: fylin@126.com

Abstract: In this paper, a surface self-cleaning wood was obtained by loading Bi₂O₃-doped silica-titanium composite film on the surface of wood by the sol-gel method. The effects of different Bi doping amounts on the structure and photocatalytic properties of the modified wood were investigated. The doping of Bi₂O₃ inhibited the growth of TiO₂ crystals and the phase transition from anatase to rutile. In addition, Bi₂O₃ could improve the photocatalytic activity of the composite film by appropriately reducing the grain size of TiO₂ and increasing the crystallinity of TiO₂. Furthermore, doping with Bi₂O₃ shifted the absorption wavelength of the wood samples back into the visible range, indicating that the increase in Bi content favoured light absorption. The wood samples loaded with Bi₂O₃-doped Si-Ti composite membranes had the best photocatalytic activity and the highest reaction rate when n (Ti):n (Bi) = 1:0.015. Degradation rates of 96.0% and 94.0% could be achieved for rhodamine B and gaseous formaldehyde, respectively. It can be seen that wood samples loaded with Bi₂O₃-doped Si-Ti composite films on the surface exhibit excellent photocatalytic activity against both gaseous and liquid pollutants.

Keywords: photocatalysis; wood surface; Bi₂O₃-doped titanium-silicon composite film; dynamics

Citation: Liu, Z.; Xu, J.; Cheng, S.; Qin, Z.; Fu, Y. Photocatalytic Performance and Kinetic Studies of a Wood Surface Loaded with Bi₂O₃-Doped Silicon–Titanium Composite Film. *Polymers* **2023**, *15*, 25. <https://doi.org/10.3390/polym15010025>

Academic Editor: Olga Klinkova

Received: 13 October 2022

Revised: 2 December 2022

Accepted: 16 December 2022

Published: 21 December 2022



Copyright: © 2022 by the authors. Licensee MDPI, Basel, Switzerland. This article is an open access article distributed under the terms and conditions of the Creative Commons Attribution (CC BY) license (<https://creativecommons.org/licenses/by/4.0/>).

1. Introduction

Wood is widely used for construction and decoration because of its beautiful surface texture and unique environmental properties. The surface of wood is not only a major factor in determining the quality, value, and price of wood products, but also the most direct and sensitive part of human senses, which is important for the processing and use of wood [1]. However, the surface of wood is not only susceptible to liquid contamination, which affects its cleanliness and aesthetics, but also to microbial attack, mould, and decay, which shortens the life of the wood. Therefore, improving the properties of wood surfaces to enhance their efficacy and extend their service life has been a popular topic of research.

Formaldehyde, causing great harm to human beings, is the main gaseous pollutant produced in the process of interior decoration, artificial board making, and furniture finishing. Further, organic dye wastewater is one of the pollutants that have always existed in the printing and dyeing industry. Currently, the common treatment methods for formaldehyde and organic wastewater include adsorption [2,3], oxidation [4,5], biological treatment [6,7], and photocatalytic method [8,9], etc. As one of the best functional materials, TiO₂ is also widely used for surface property improvement of wood due to its excellent chemical stability and non-toxicity. In water and air systems, TiO₂ can be excited by UV light to generate photovoltaic electronics and holes and form highly chemically active radicals and reactive oxygen species on the surface. Therefore, it can react with most organic substances and decompose them into CO₂ and H₂O, resulting in the degradation of organic pollutants [10]. As early as 2002, Okawa et al. [11] prepared wood/TiO₂ composites for the photocatalytic degradation of organic matter. Subsequently, Xia et al. [12] described the research progress

of nano titanium dioxide photocatalytic modification from the reaction mechanism of nanotitanium dioxide photocatalytic degradation of formaldehyde and rationalized the feasibility of nanotitanium dioxide application in wood industry. Fu et al. [13] achieved photocatalytic degradation of the azo dye AO7 by $\text{SiO}_2/\text{TiO}_2$ modified materials prepared by a sol-gel method. Ag-TiO₂ composite film-loaded wood capable of catalytic degradation of phenol under visible light irradiation was prepared by hydrothermal and silver mirror reactions by L. Gao [14] and L. Kun Gao [15], respectively. The former still had high photocatalytic activity after hydrophobic treatment, which provides a new possibility for the preparation of self-cleaning wood products.

In general, TiO₂ has photocatalytic activity only under ultraviolet light, which is only a small fraction of sunlight. However, the wavelengths of light sources for indoor lighting are usually in the visible light range, which certainly limits the practical use and scope of TiO₂-modified wood. Therefore, visible photocatalytic modification of TiO₂ by elemental doping, noble metal deposition, semiconductor compounding, and ion doping is needed to broaden its photoreaction range and inhibit the compounding of photogenerated electrons-hole, resulting in the improvement of its photocatalytic activity. The forbidden band width of semiconductor Bi₂O₃ is 2.8 eV, which is narrower than that of TiO₂, and therefore its absorption wavelength is longer. In addition, it has been shown [16–20] that Bi₂O₃ compounded with TiO₂ can improve the photocatalytic activity of TiO₂ and make it responsive in visible light. Therefore, a sol-gel method was used to load Bi₂O₃-doped silica-titanium composite films on the wood surface to improve the self-cleaning properties of the wood, and the effects of different Bi doping amounts on the surface morphology, chemical structure, crystal structure, and surface photocatalytic properties of the modified composite films were investigated.

2. Materials and Methods

2.1. Materials

Tsoongiodendron odorum wood was selected as test material, which was collected from Liangfengjiang National Forest Park, Nanning, Guangxi, China. The air-dried test material was processed into a 40 mm (L) × 40 mm (T) × 5 mm (R) sample size. The sample with a smooth surface and no defect was cleaned with distilled water and air-dried indoors (moisture content was about 15%) for later use.

2.2. Preparation of Composite Films

With the ratio of n (TBOT):n (EtOH):n (VETS):n (H₂O):n (HNO₃) being 1:5:0.2:1:0.5, the mixture of VETS and 1/3 EtOH were added to the mixture of TBOT and 1/3 EtOH under magnetic stirring, and then the mixture of 1/3 EtOH, H₂O and HNO₃ was added, and stirred vigorously for 10 min to obtain liquid A. BiCl₃ was weighed at the molar ratio of n (Ti):n (Bi) (1:0, 0.005, 0.0075, 0.01, 0.015, 0.02) and dissolved in 0.2 mol of anhydrous ethanol and 0.1 mol of nitric acid mixture, respectively, and stirred vigorously for 10 min to obtain liquid B. Under vigorous stirring, liquid B was slowly dripped into liquid A and continued to be stirred for 1 h, then left at room temperature to form a sol. The sol was applied evenly to the surface of the wood and left for 1 h before a second application was made. After aging for 24 h, the wood was dried in a constant temperature oven at 100 °C for 6 h and then cooled to room temperature to obtain a series of wood samples with Bi²O³-doped silica-titanium composite films loaded on the surface, and the wood specimens loaded with different bismuth doping amounts (0.005, 0.0075, 0.01, 0.015, 0.02) of silica-titanium composite films were noted as BSTX, X = 0, 1, 2, 3, 4, 5.

2.3. Characterization of BSTX

2.3.1. Morphology and Structural Characterization of Wood Surface

The surface morphology of Bi₂O₃-doped silicon titanium composite film on the wood surface was observed by stereomicroscope. A 300 kV emission transmission electron microscope was used to observe the lattice parameters of crystalline particles and judge their

crystal structure. In this paper, the chemical structure of SiO₂ and TiO₂ in the composite film and its bonding mode with wood surface were analyzed by a Nicoletis 50 Fourier transform infrared spectrometer (Waltham, MA, USA). The crystallinity and crystal structure of SiO₂ and TiO₂ in the silicon titanium composite film were analyzed by a dX-2700A high-power (4 kW) polycrystalline X-ray diffractometer. The UV-visible diffuse reflectance spectra of the silica–titanium composite films doped with Bi₂O₃ on the wood surface were tested by UV-2501PC UV-visible spectrophotometer (Kyoto, Japan). BaSO₄ was used as a reference, and the scanning range was 250–800 nm. The light emitted from the light source was processed into a sample of wood loaded with a bismuth-doped silica–titanium composite film and passed through an integrating sphere with an inner wall coated with BaSO₄. The reflected light from the surface of the sample was collected and projected back to the receiver, where an electrical signal was generated and recorded on the recorder as a function of wavelength, resulting in a spectral curve. The band gaps of the samples were calculated using the Tauc equation (Equation (1)) based on the UV diffuse reflectance spectroscopy data [21].

$$(\alpha h\nu)^{1/2} = A(h\nu - E_g) \quad (1)$$

where h is Planck's constant, ν is frequency of vibration, α is absorption coefficient, E_g is band gap, and A is proportional constant.

2.3.2. Characterization on Photocatalytic Performance

The photocatalytic performance of wood samples was evaluated by catalytic degradation of rhodamine B aqueous solution and gaseous formaldehyde under visible light.

Degradation of Rhodamine B: The standard curve of absorbance of rhodamine B aqueous solution changing with concentration was shown in Figure 1. A 500 W xenon lamp ($\lambda > 420$ nm) was selected as the light source, and a glass beaker was used as the reactor to immerse the wood sample with a Bi₂O₃-doped silica–titanium composite film into 30 mL of rhodamine B solution at a concentration of 10 mg/L. The samples were placed in the dark for 30 min and the concentration of Rhodamine B was determined as the initial concentration C_0 after adsorption equilibrium was reached. The lamp was then turned on so that the surface of the wood with the composite film faced the light source vertically. The effective area of the wood sample was 40 mm × 40 mm, and the distance from the center of the light source was 40 cm. The reaction temperature was controlled at 20–30 °C. The illumination time was 180 min, and samples were taken every 30 min. The degradation rate of Rhodamine B was calculated by measuring the absorbance at the wavelength of 554 nm and converting it into concentration C . In the blank control group, wood samples without Bi₂O₃ doping were added. The decolorization rate D was calculated by the following equation.

$$D = [(C_0 - C)/C_0] \times 100\% \quad (2)$$

Degradation of the gas formaldehyde: The formaldehyde standard solution with a mass fraction of 0.02 mg/mL was first configured. Then, 3 mL of the formaldehyde standard solution was converted into gas through the formaldehyde generator into the reaction device (Figure 2). The concentration of formaldehyde gas in the reaction chamber was measured with a formaldehyde detector after 30 min of adsorption in the dark as the initial concentration C_0 . The light was then turned on, keeping the wood surface with the composite film vertically facing the light source. The effective area of the wood sample was 40 mm × 40 mm, and the distance from the center of the light source was 40 cm. The reaction temperature was controlled at 20–30 °C and the illumination time was 180 min. The formaldehyde gas concentration in the reaction box was detected by a formaldehyde detector every 30 min. In blank control group, wood samples without Bi₂O₃ doping were added. The calculation of degradation rate D was the same as Formula (1).

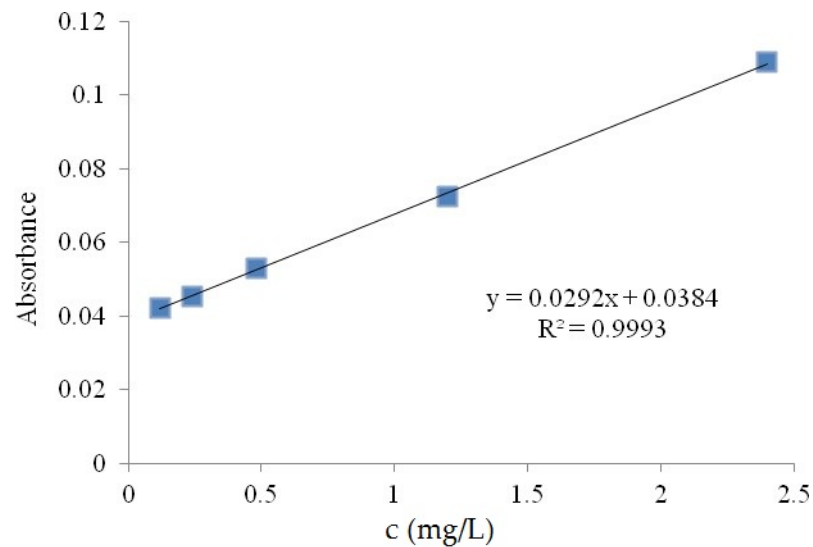


Figure 1. The standard curve of Rhodamine B aqueous solution.

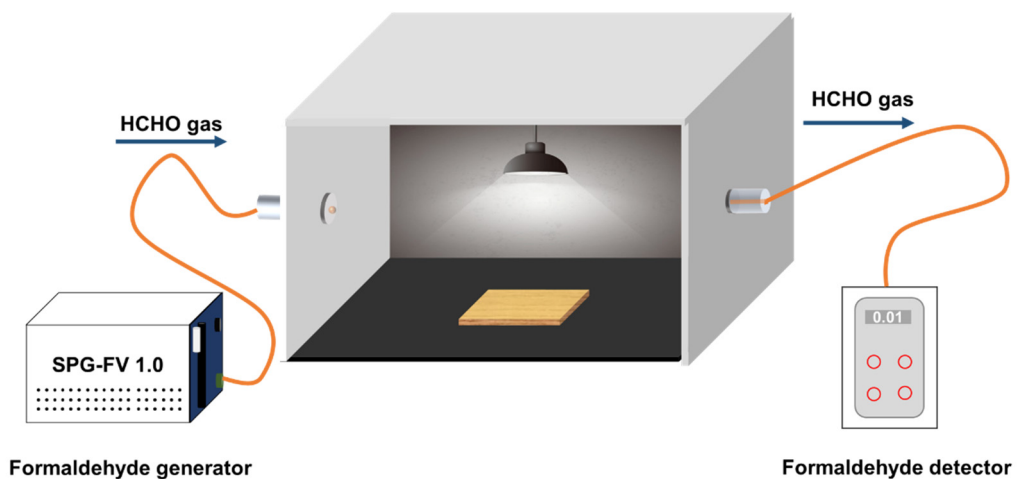


Figure 2. Reaction device for the photocatalytic degradation of formaldehyde.

2.3.3. Photocatalytic Reaction Kinetic Model

The occurrence of a reaction, the direction of the reaction, and the concentration of substances involved in the reaction all depends on thermodynamics. Further, kinetics can be used to describe the reaction rate, the sequence of steps in the reaction, and the factors controlling the reaction rate. According to research, there are mainly two forms of photocatalytic reaction kinetics model: (1) Langmuir-Hinshelwood model (L-H model for short) [22], (2) Power law model [23].

In the L-H model, the reaction rate R is proportional to the reactant coverage θ on the membrane surface.

$$R = k\theta = \frac{kKC}{1 + KC} \quad (3)$$

where, k is the reaction rate constant, mol/min; K is the absorption coefficient of reactants on the membrane surface, m^3/mol ; C is the reactant concentration. When C is very small, $KC \ll 1$, Formula (3) can be reduced to Equation (4) as shown below.

$$R = kKC \quad (4)$$

Equation (4) is the kinetic equation of the first order reaction. First integrate this equation, when the initial reaction $t = 0$, $C = C_0$ (C_0 is the initial reaction concentration, C is the reaction concentration at time t), then the following equation can be obtained.

$$-\ln C/C_0 = k_{app}t = kKt \quad (5)$$

2.3.4. Surface Wettability Test

The wettability of the solid surface is generally expressed by the contact angle θ of the liquid on the solid surface. If $0^\circ < \theta < 90^\circ$, the solid surface is hydrophilic; if $90^\circ < \theta < 180^\circ$, the solid surface is hydrophobic; and the larger θ is, the better the hydrophobicity of the solid surface is. In this paper, the static contact angle of distilled water on the wood surface was measured by a DSA100E Klux contact angle meter (Hamburg, Germany), the volume of water droplets was $5 \mu\text{L}$, the contact angle of water droplets stayed on the wood surface for 10 s, the test temperature was $20 \pm 1^\circ\text{C}$, and the relative humidity was $65 \pm 3\%$. Overall, 5 points were tested for each sample and 3 samples were tested for each treatment. Finally, the average value was taken as the contact angle on the surface of wood.

3. Results and Discussion

3.1. Analysis of Wood Surface Morphology

According to the stereoscopic microscope view (magnification $28.5\times$) in Figure 3, a layer of yellow film was loaded on the treated wood surface, while some cracks appeared in the composite film after doping with Bi_2O_3 . Combined with Figure 4, it may be due to the poor combination of Bi_2O_3 loaded on the wood surface with TiO_2 and SiO_2 , and cracks due to different shrinkage, stress, and thermal expansion coefficients between particles and wood matrix during drying, which may be the reason for the decrease in contact angle [24].

3.2. FTIR Analysis

Figure 4 shows the FTIR patterns of samples with different Bi doping amounts. From the figure, it can be seen that doping of Bi_2O_3 makes some changes in the chemical groups of Si-Ti composite film on the wood surface. The broad and obtuse peak near 3415 cm^{-1} was the stretching vibration peak of -OH, partly from -OH in wood cellulose and partly from -OH produced by the hydrolysis of TBOT and VETS during the reaction. The peaks near 2921 cm^{-1} and 2850 cm^{-1} were the stretching vibration peaks of C-H in $-\text{CH}_2$, which may come from the incomplete hydrolysis residue of wood cellulose, TBOT, and VETS, but the strength was very weak, so it was speculated that the hydrolysis reaction was sufficient and the residual $-\text{CH}_2$ was lessened. The peak near 1631 cm^{-1} may be the stretching vibration peak of C=C, and its vibration intensity decreased with the increase in the content of Bi_2O_3 . It was speculated that the doping of Bi_2O_3 would hinder the loading of $-\text{CH}=\text{CH}_2$ on the wood surface, which may be the reason for the decrease in contact angle. The peak near 1550 cm^{-1} detected when $n(\text{Ti}):n(\text{Bi}) \geq 1:0.005$ may be the stretching vibration peak of Bi-O, the peak near 1300 cm^{-1} detected by $n(\text{Ti}):n(\text{Bi}) \geq 1:0.075$ may be the stretching vibration peak of Bi-O [25], and the intensity of the vibration peak increased with the increase in the amount of Bi doping. It was speculated that Bi_2O_3 may be formed in the reaction. The sharp peak of 1380 cm^{-1} was the stretching vibration peak of $-\text{NO}_3$. The peaks near 1120 cm^{-1} and 1030 cm^{-1} may be Si-O-Si asymmetric stretching vibration peaks. The peak near 900 cm^{-1} may be the stretching vibration of Ti-O-Si, but the peak strength was weak and not obvious, suggesting that the binding between TiO_2 and SiO_2 was weak. The peak near 560 cm^{-1} may be the stretching vibration peak of Ti-O-Ti. The appearance of Si-O-Si and Ti-O-Ti indicated that TiO_2 and SiO_2 were successfully supported on the wood surface.

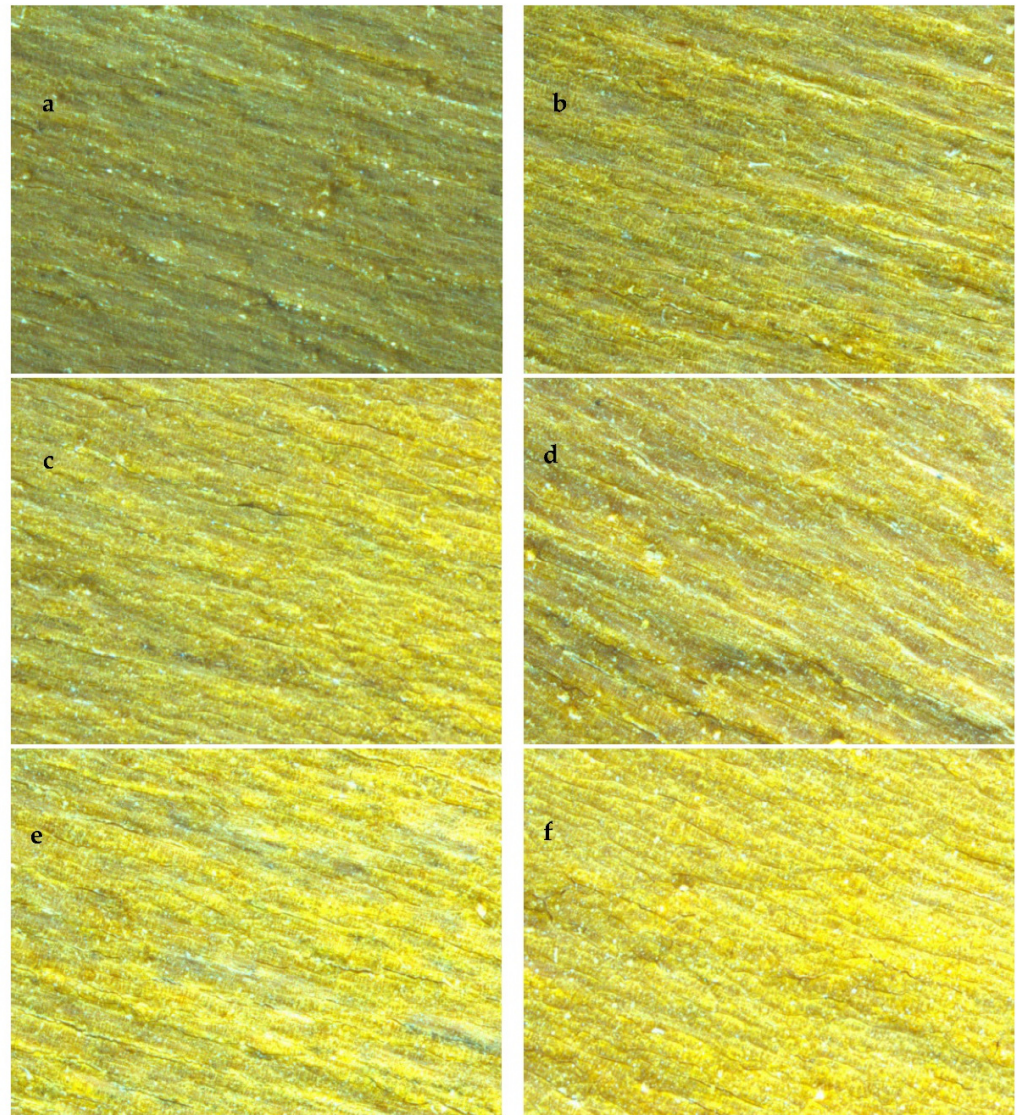


Figure 3. The stereoscopic microscope image of Si–Ti composite film prepared at different Bi_2O_3 -doped amounts. ((a–f) are the stereoscopic microscope image of BST0, BST1, BST2, BST3, BST4, BST5).

3.3. Analysis of Crystallinity and Crystal Structure

Figure 5 shows the XRD patterns of composite films on the surface of wood samples with different Bi doping levels. According to the figure analysis, when Bi was not doped, the composite film was mainly composed of anatase TiO_2 , but a small peak of rutile TiO_2 appears at $2\theta = 69.008^\circ$. After doping with Bi, the small peak of rutile TiO_2 changed slightly, especially at the higher doping amount of bismuth where the peak basically disappeared, indicating that the composite film was composed of anatase TiO_2 at this time. It can be concluded that the doping of Bi_2O_3 can inhibit the phase change of TiO_2 from anatase to rutile in a certain extent. In addition, with the increase in Bi doping amount, the position of the TiO_2 peak did not shift, and no new peak was generated, indicating that Bi and Ti did not generate new composite oxides. The average grain size of the BSTX composite film was calculated by the Scheler formula and the half-peak width of the anatase TiO_2 (101) crystal plane. The results were shown in Table 1.

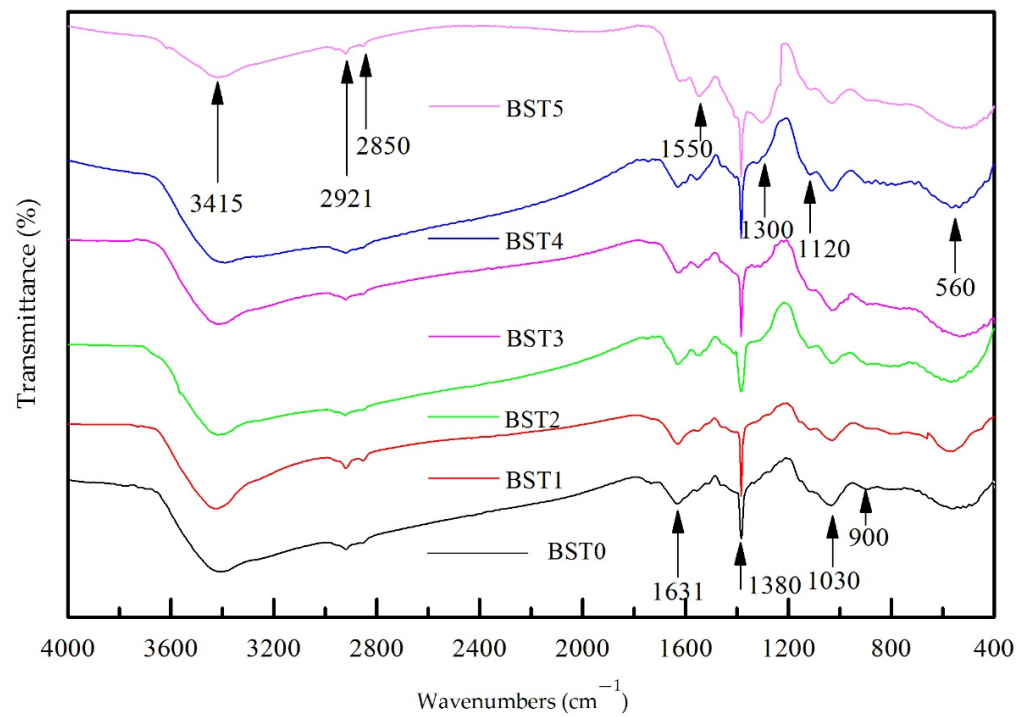


Figure 4. The FTIR spectrum of Si-Ti composite film prepared at different Bi-doped amounts.

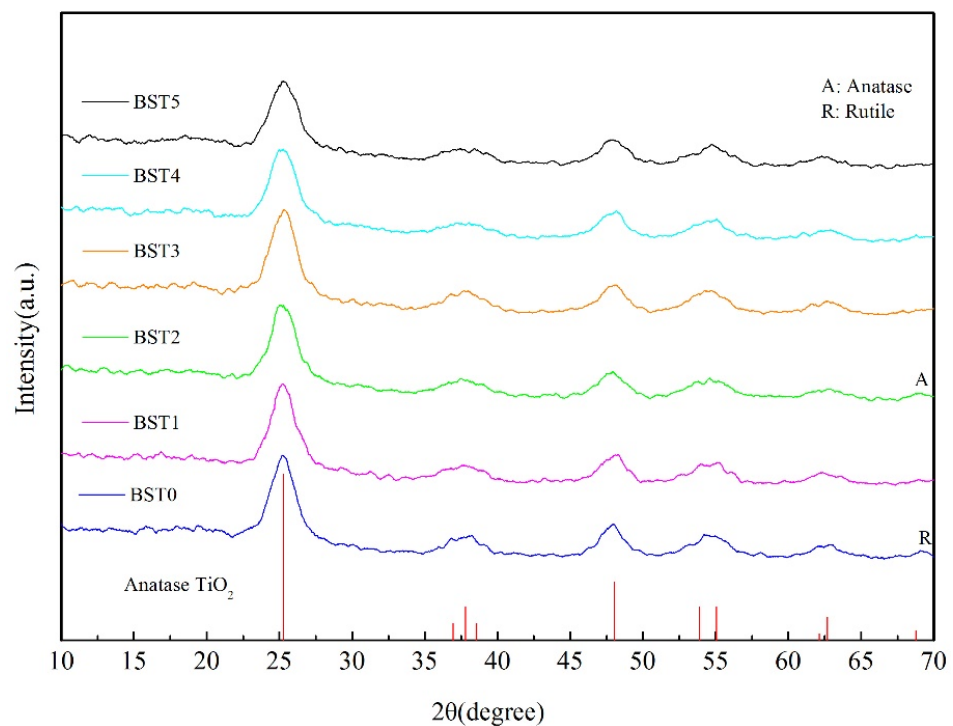


Figure 5. The XRD spectrum of Si-Ti composite film prepared at different Bi-doped amounts.

Table 1. The average crystal grain size of Bi-Ti/Si-X composite film.

	ST0	BST1	BST2	BST3	BST4	BST5
Grain size/nm	93.49	87.65	82.27	76.94	71.77	56.19
Crystallinity/%	56.54	59.55	60.77	61.34	70.82	65.28

The TiO₂ microstructure such as energy band structure, degree of crystallinity, and crystal particle size may affect the photocatalytic activity of TiO₂ [26]. It can be seen from Table 1 that with the increase in Bi doping amount, the average grain size of TiO₂ decreased, indicating that Bi₂O₃ inhibits the growth of TiO₂ crystals, which was consistent with previous studies [27]. In addition, the best photocatalytic efficiency of BST4 can be seen in Figures 6 and 7, indicating that the reduction in crystal size within a certain range is beneficial for the increase in photocatalytic activity. With the increase in Bi doping amount, the crystallinity of TiO₂ increased first and then decreased. When n(Ti):n(Bi) = 1:0.015, the crystallinity of TiO₂ was the highest. The higher the crystallinity of the crystal, the fewer the internal defects and the corresponding reduction in the chance of electron-hole recombination; the high crystallinity would promote the rapid transfer of photo-generated electrons from the inside of the crystal to the surface, effectively inhibiting the photo-generated electron-hole recombination, thereby improving the quantum efficiency of photocatalysis and enhancing the photocatalytic activity [27].

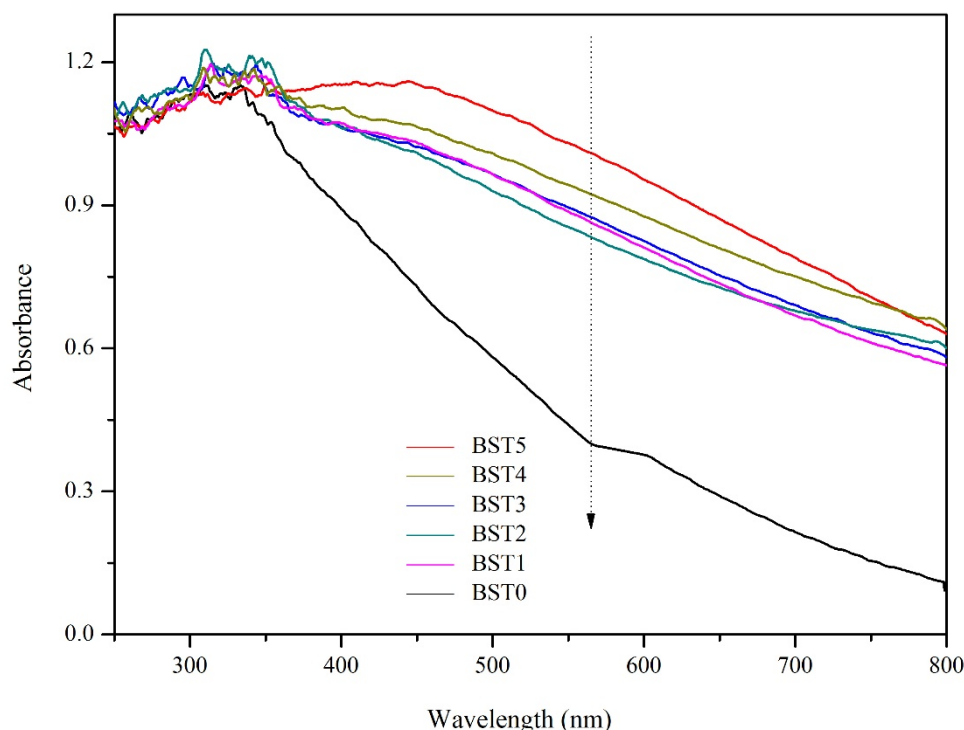


Figure 6. UV-Vis spectrum of Si–Ti composite film prepared at different Bi-doped amounts.

The HRTEM photo of the film layer on the surface of wood sample with n(Ti):n(Bi) = 1:0.015 is shown in Figure 8. As can be seen from the figure, clear lattice stripes can be seen in the BST3 sample. The spacing of these lattice stripes was 0.352 nm, corresponding to the 101 crystal plane of AnataseTiO₂, which was consistent with the results of the XRD test. Although the stripes with lattice spacing of 0.331 nm correspond to the 111 crystal plane of α -Bi₂O₃, these lattice stripes were vague, which may be due to the small amount of Bi₂O₃ or the low crystallinity.

3.4. UV-VIS Diffuse Reflectance Spectrum Analysis

Figure 6 shows the absorption spectrum calculated from the UV-vis diffuse reflection spectrum according to the Kubelka Munk (km) theory. As can be seen from Figure 6, the difference in absorption intensity of silicon–titanium composite film with different Bi doping amount was very small—between 250 nm–350 nm. The main absorption wavelength of wood loaded with silicon–titanium composite film was below 400 nm, while the wood coated with silicon–titanium composite film doped with Bi₂O₃ had strong light absorption

capacity within the range of 400–800 nm. This indicated that the absorption wavelength of wood samples were red-shifted to the visible light range after Bi_2O_3 doping. As the Bi doping content increased, the light absorption ability of wood samples in the range of 400–800 nm was enhanced, indicating that the increase in Bi content was beneficial to light absorption, because the light response in the visible region was mainly from the photosensitization of Bi_2O_3 [28].

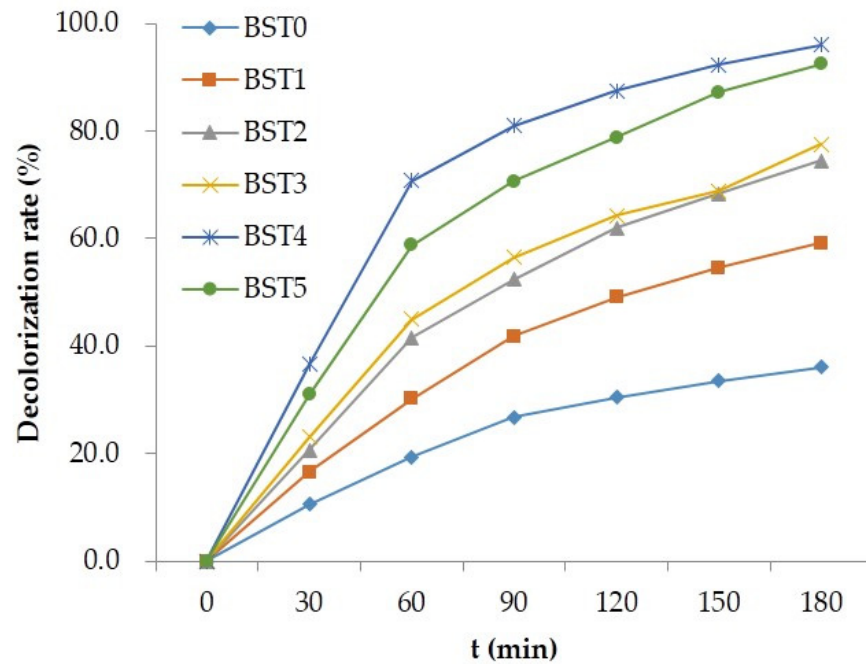


Figure 7. The decolorization rate of Rhodamine B from different Bi-doped wood samples.

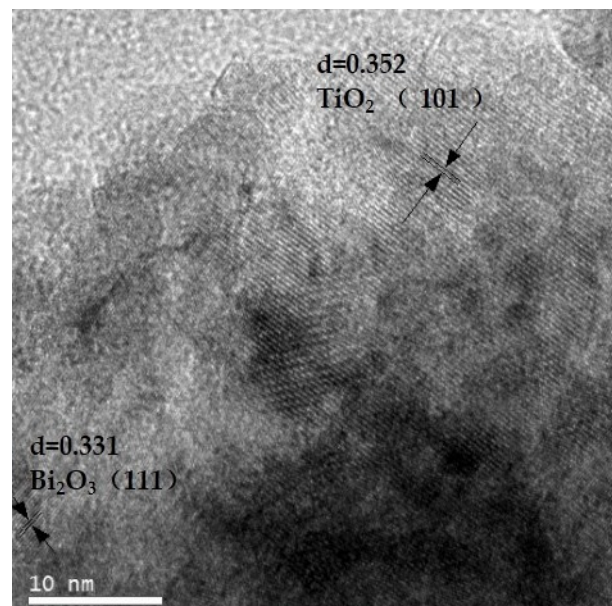


Figure 8. HRTEM image of Si-Ti composite film surface of the BST5 sample.

As shown in the Table 2, the band gaps of the Si-Ti composite films without Bi doping and with Bi doping were 1.56, 1.36, 1.41, 1.34, 1.25, and 1.35 eV, respectively. It can be seen that the band gap of titanium dioxide in the Si-Ti composite film is reduced after doping with Bi, which makes the material absorb less light and shift toward the infrared direction,

which will be beneficial to the improvement of the visible photocatalytic performance of the composite film. In addition, the decolorization and removal rates of BST4 for rhodamine B and formaldehyde (Figures 7 and 9) were 96% and 94%, respectively, which indicated that the reduction in band gap had a certain promotion effect on the photocatalytic performance of the composite film.

Table 2. The band gaps of Bi-Ti/Si-X composite films.

	ST0	BST1	BST2	BST3	BST4	BST5
Eg (eV)	1.56	1.36	1.41	1.34	1.25	1.35

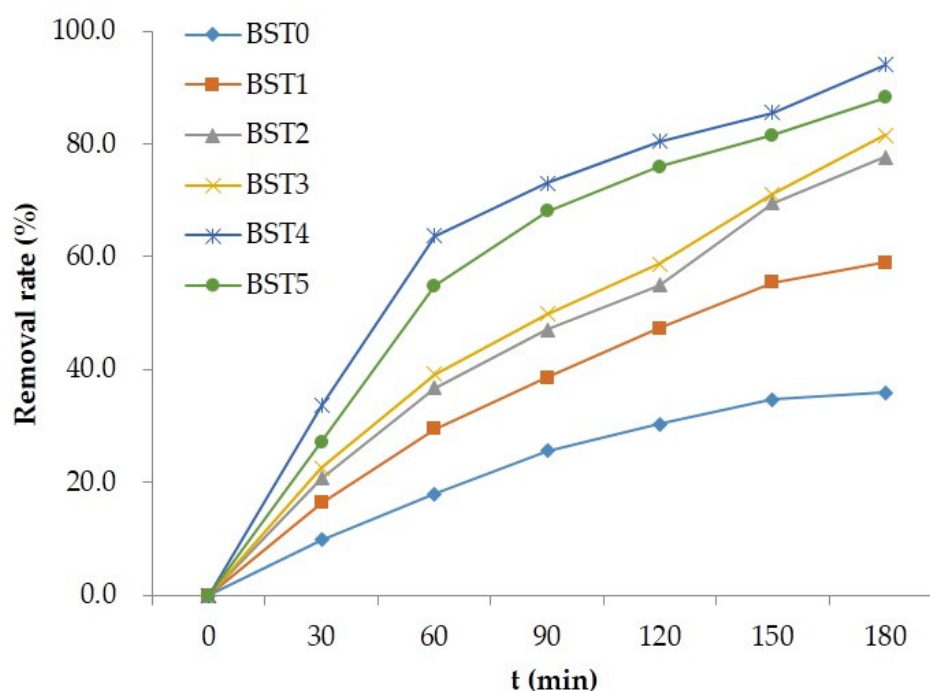


Figure 9. The removal rate of gas Formaldehyde in different Bi-doped wood samples.

3.5. Analysis of Photocatalytic Activity

The photocatalytic activity of Si-Ti composite film on the wood surface before and after Bi₂O₃ doping was evaluated by using liquid phase degradation of rhodamine B and gas phase degradation of formaldehyde under visible light as probe reaction. Figure 7 shows the degradation of Rhodamine B aqueous solution by wood samples loaded with different Bi₂O₃ doped silicon titanium composite films under visible light irradiation. It can be seen from the figure that under visible light irradiation, the photocatalytic activity of wood samples doped with Bi₂O₃ was obviously better than that of wood samples without Bi₂O₃, in which n (Ti):n (Bi) = 1:0.015 had the highest photocatalytic activity, and the decolorization rate of rhodamine B was 96.0%. Combining Figures 7 and 8, it can be seen that the photocatalytic activity of wood samples loaded with Bi₂O₃-doped Si-Ti composite films depended on the amount of Bi doping, but excessive Bi content led to the agglomeration of Bi₂O₃, which became a photoelectron-hole recombination center and reduced the quantum efficiency, thus weakening the photocatalytic activity [29].

The wood samples loaded with Bi₂O₃-doped Si-Ti composite films showed excellent photocatalytic activity not only in the degradation of liquid phase dyes, but also in the removal of gaseous pollutant formaldehyde. As shown in Figure 8, similar to the result of degradation of rhodamine B, when n (Ti):n (Bi) = 1:0.015, the wood sample loaded with Bi₂O₃-doped silicon-titanium composite film had the best photocatalytic activity, with the removal rate of formaldehyde reaching 94.0%.

3.6. Analysis of Reaction Kinetics

It can be seen from Equation (5) that if $\ln C/C_0$ was used to plot the reaction time T , a straight line should be obtained [30]. The reaction kinetics curves of photocatalytic degradation of rhodamine B and gaseous formaldehyde by Si-Ti composite film loaded on the wood surface with different Bi doping amount were obtained by plotting and fitting $\ln C/C_0$ to reaction time T , as shown in Figures 10 and 11. It can be seen from the figure that the fitted $\ln C/C_0 \sim t$ was in a straight line, with the minimum R^2 of 0.9587 and the maximum R^2 of 0.9952, and that the fitting degree was high, indicating that the photocatalytic oxidation reaction of rhodamine B and formaldehyde on the surface of silicon titanium composite film with different Bi doping amount conforms to first-order reaction kinetics when rhodamine B and formaldehyde concentration were adsorbed on the surface. Therefore, in the photocatalytic degradation of rhodamine B and formaldehyde by silicon-titanium composite film with different Bi doping levels, the speed of the photocatalytic reaction on the surface of the composite film controlled the overall reaction rate rather than the adsorption process, indicating that the photocatalytic oxidation reaction rate of the composite film only depended on the speed of the photocatalytic reaction [31].

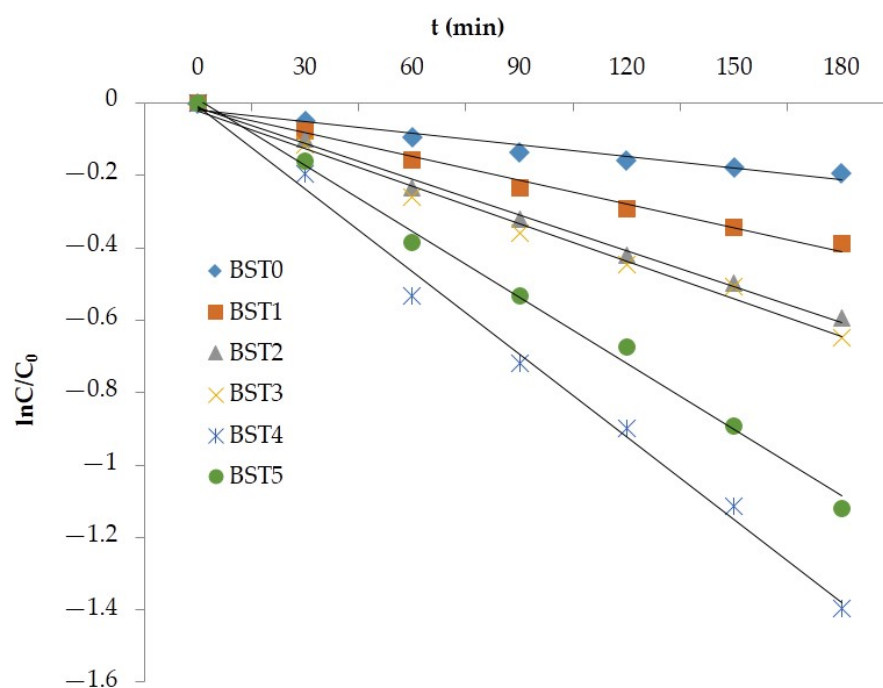


Figure 10. The reaction kinetics curves of degradation of RhB in different Bi-doped levels of wood samples.

Figure 12 shows the apparent reaction rate constant of degradation of rhodamine B and gaseous formaldehyde by Si-Ti composite films with different Bi doping amounts. As can be seen from the figure, with the increase in the amount of Bi doping, the change trend of the apparent reaction rate constant of the composite film to rhodamine B and gas formaldehyde was the same, which increased at first and then decreased. The apparent rate constants of the composite films for rhodamine B and gaseous formaldehyde were equal at $n(\text{Ti}):n(\text{Bi})$ of 1:0 and 1:0.005. When $n(\text{Ti}):n(\text{Bi})$ was 1:0.0075 and 1:0.01, the apparent reaction rate constant of the composite film for degrading gaseous formaldehyde was larger than that of rhodamine B. In contrast, the apparent reaction rate constants for the degradation of rhodamine B by the composite films were greater than that of formaldehyde when $n(\text{Ti}):n(\text{Bi})$ was 1:0.015 and 1:0.02. Moreover, the Si-Ti composite film doped with Bi^2O^3 at $n(\text{Ti}):n(\text{Bi})$ of 1:0.015 showed the highest degradation rates of 0.2283 and 0.1877 for rhodamine B and gaseous formaldehyde, respectively.

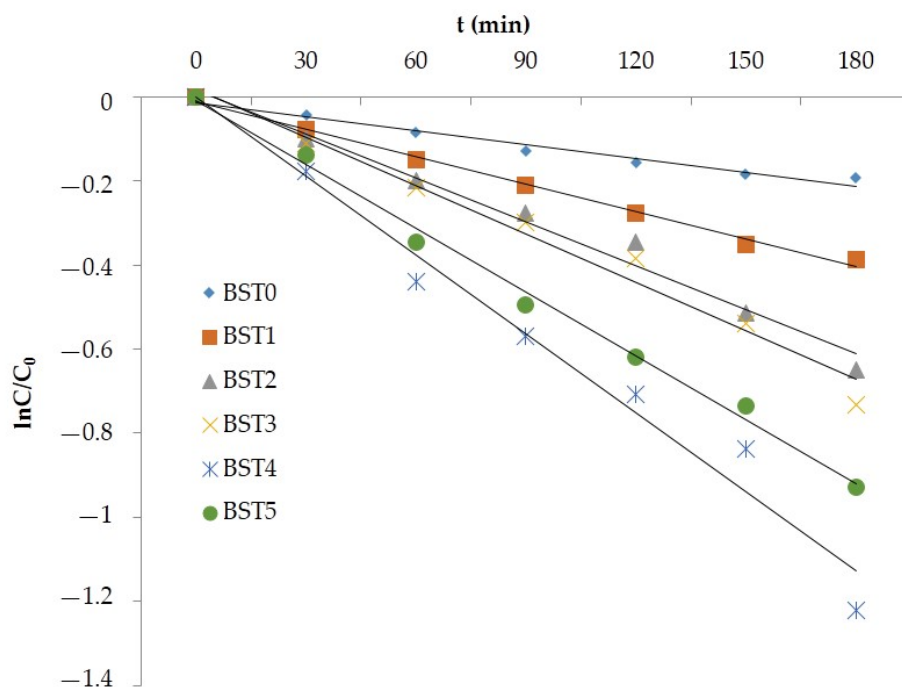


Figure 11. The reaction kinetics curves of degradation of Gaseous formaldehyde in different Bi-doped levels of wood samples.

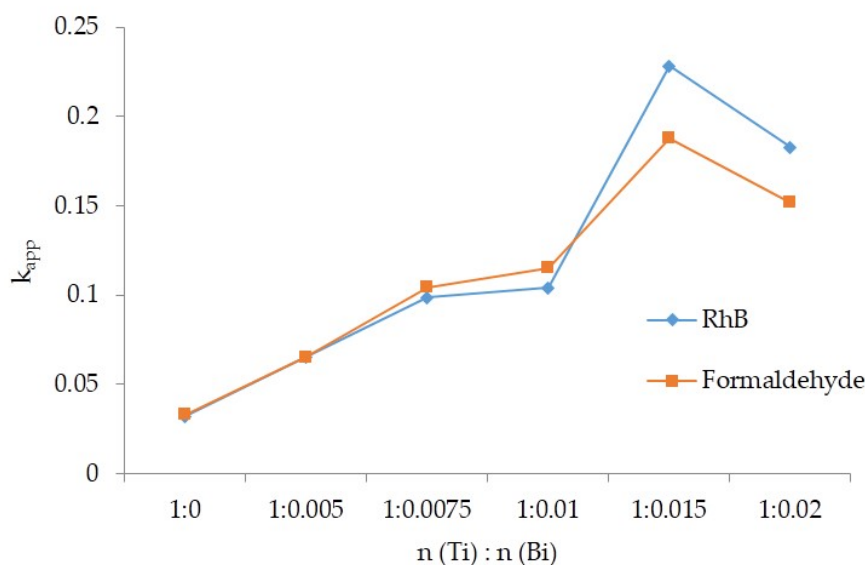


Figure 12. The rate constant of the apparent reaction of RhB and Gas Formaldehyde degraded by different Bi doping Si-Ti composite films.

3.7. Analysis of Surface Wettability

The contact angles of silica-titanium composite films with different Bi doping amounts were shown in Figure 13. It can be seen from the figure that the contact angle of the wood specimens showed a decreasing trend with the increase in Bi doping amount; when the doping amount increased from 0 to 2%, the contact angle decreased from 125.9° to 91.4°, indicating that the increase in Bi₂O₃ would reduce the hydrophobicity of the silica-titanium composite film on the wood surface. Combined with the surface morphology and FTIR results, it was speculated that it may be due to the fact that the Bi₂O₃ loading on the surface of the wood increased with the increase in Bi doping. Alternatively, Bi₂O₃ did not bond

well with TiO_2 and SiO_2 , and cracks occurred during the drying process due to different drying stresses between the particles as well as between the wood [24]. Furthermore, the doping of Bi_2O_3 may hinder the loading of $-\text{CH}=\text{CH}_2$ on the wood surface and thus the hydrophobic group decreases, leading to a decrease in hydrophobicity.

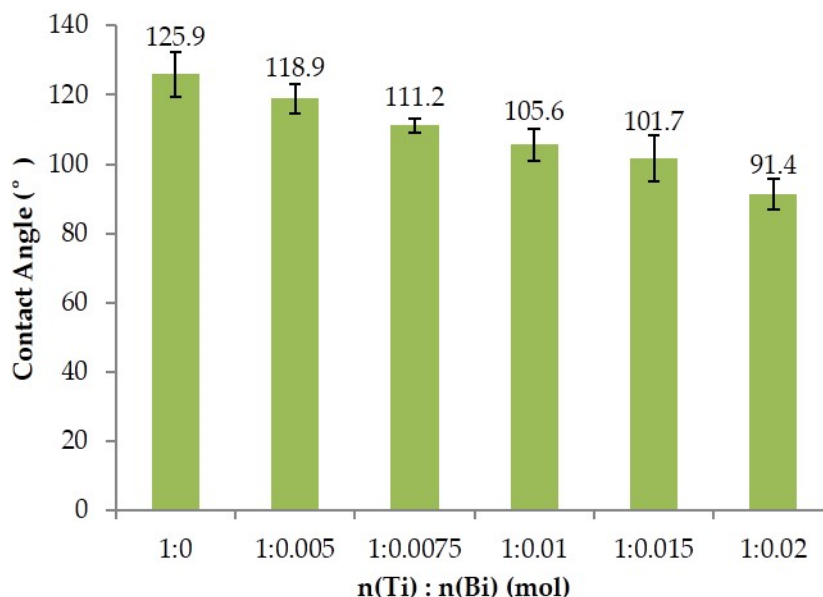


Figure 13. The contact angle of Si-Ti composite film prepared at different Bi-doped amounts.

4. Conclusions

Wood samples loaded with Bi_2O_3 -doped Si-Ti composite films were prepared by a sol-gel method in this paper. It can be inferred from the appearance of the Bi-O stretching vibration peaks that the wood surface was successfully loaded with Bi_2O_3 , and the doping of Bi_2O_3 affected the loading of $-\text{CH}=\text{CH}_2$ on the wood surface, which may be the reason for the decrease in contact angle. The doping of Bi_2O_3 inhibited the growth of TiO_2 crystals and the phase transition from anatase to rutile. In addition, Bi_2O_3 reduced photoelectron-hole recombination by reducing the grain size of TiO_2 and increasing the crystallinity of TiO_2 , which improved the photocatalytic activity. In addition, the reduction in TiO_2 band gap after doping with Bi_2O_3 shifted the absorption wavelength of wood samples to the visible range, indicating that the increase in Bi content was beneficial to light absorption. The wood samples loaded with Bi_2O_3 -doped silica-titanium composite films had the best photocatalytic activity and the highest reaction rate when $n(\text{Ti}):n(\text{Bi}) = 1:0.015$. The degradation rates of Rhodamine B and gaseous formaldehyde could reach 96.0% and 94.0%, respectively. The contact angle test showed that the contact angle of the wood samples decreased with increasing Bi content after doping with Bi_2O_3 , which might be due to the reduction in cracks and hydrophobic groups on the surface of the composite film.

Author Contributions: Y.F. conceived and designed the experiments; S.C. and J.X. drafted the manuscript; Z.L. and S.C. participated in data analysis; S.C. and J.X. carried out the laboratory work; Z.Q. and Z.L. were responsible for the revision and editing of the thesis. All authors gave final approval for publication. All authors have read and agreed to the published version of the manuscript.

Funding: This research was funded by Guangxi Forestry Science and Technology Project, Guilin Scientific Research [2021]20 and the Special Fund of the National Natural Science Foundation of China (Grant number 31870540).

Institutional Review Board Statement: Not applicable.

Data Availability Statement: Not applicable.

Acknowledgments: The authors gratefully acknowledge financial support from Guangxi Forestry Science and Technology Project, Guilin Scientific Research [2021]20 and the Special Fund of the National Natural Science Foundation of China (31870540). And we are very grateful for the assistance provided by the Large Scale Instrument Sharing Platform of Guangxi University in the characterization of the structure and properties of composite films.

Conflicts of Interest: The authors declare no conflict of interest.

References

1. Li, J.; Duan, X.; Liu, Y. Functional modification of wood surfaces. *J. Northeast. For. Univ.* **1995**, *23*, 95–101. [[CrossRef](#)]
2. Becker, A.; Israfilov, N.; Ehrstein, E.; Lara-Ibeas, I.; Planeix, J.-M.; Louis, B.; Le Calvé, S. Adsorption of gaseous formaldehyde on Y zeolites and on metal-organic frameworks. *Micropor. Mesopor. Mat.* **2022**, *343*, 112136. [[CrossRef](#)]
3. Qiu, B.; Shao, Q.; Shi, J.; Yang, C.; Chu, H. Application of biochar for the adsorption of organic pollutants from wastewater: Modification strategies, mechanisms and challenges. *Sep. Purif. Technol.* **2022**, *300*, 121925. [[CrossRef](#)]
4. Qiang, W.-J.; Huang, Q.; Shen, J.-H.; Ke, Q.-F.; Lü, J.-Y.; Guo, Y.-P. Copper oxide and manganese dioxide nanoparticles on corrugated glass-fiber supportors promote thermocatalytic oxidation of formaldehyde. *J. Clean. Prod.* **2022**, *368*, 133089. [[CrossRef](#)]
5. Zhao, Y.; Wang, Y.; Chi, H.; Zhang, Y.; Sun, C.; Wei, H.; Li, R. Coupling photocatalytic water oxidation on decahedron BiVO₄ crystals with catalytic wet peroxide oxidation for removing organic pollutions in wastewater. *Appl. Catal. B* **2022**, *318*, 121858. [[CrossRef](#)]
6. Méndez, J.O.; Melián, J.H.; Araña, J.; Rodríguez, J.D.; Díaz, O.G.; Peña, J.P. Detoxification of waters contaminated with phenol, formaldehyde and phenol–formaldehyde mixtures using a combination of biological treatments and advanced oxidation techniques. *Appl. Catal. B* **2015**, *163*, 63–73. [[CrossRef](#)]
7. Dai, B.; Peng, Y.; Zhang, M.; Yang, M.; Wu, Y.; Guo, X. Insight into the effects of biological treatment on the binding properties of copper onto dissolved organic matter derived from coking wastewater. *Ecotoxicol. Environ. Saf.* **2022**, *238*, 113567. [[CrossRef](#)]
8. Liu, S.; Lin, W. A simple method to prepare g-C₃N₄-TiO₂/waste zeolites as visible-light-responsive photocatalytic coatings for degradation of indoor formaldehyde. *J. Haz. Mat.* **2019**, *368*, 468–476. [[CrossRef](#)]
9. Sibhatu, A.K.; Weldegebriela, G.K.; Sagadevan, S.; Tran, N.N.; Hessel, V. Photocatalytic activity of CuO nanoparticles for organic and inorganic pollutants removal in wastewater remediation. *Chemosphere* **2022**, *300*, 134623. [[CrossRef](#)]
10. Zu, Y.; Li, X.; Qu, X. Photocatalytic properties and applications of titanium dioxide nanoparticles. *Titanium Ind. Prog.* **1999**, *4*, 23–26. [[CrossRef](#)]
11. Okawa, S.; Sugi, S.; Oishi, H.; Watanabe, Y.; Mori, T.; Shigematsu, M.; Tanahashi, M. Improvement of wood surface by inorganic modification. *Trans. Mater. Res. Soc. Jpn.* **2002**, *27*, 637–640.
12. Xia, S.; Li, L.; Li, J. Research progress of anti-bacterium and degradation of formaldehyde by Nano-TiO₂ photo-catalysis. *Wood Process. Mach.* **2007**, *18*, 36–40. [[CrossRef](#)]
13. Fu, Y.; Liu, X.; Cheng, F.; Sun, J.; Qin, Z. Modification of the Wood Surface Properties of *Tsoongiodendron odorum* Chun with Silicon Dioxide by a Sol-gel Method. *Bioresources* **2016**, *11*, 10273–10285. [[CrossRef](#)]
14. Gao, L.; Gan, W.; Xiao, S.; Zhan, X.; Li, J. A robust superhydrophobic antibacterial Ag-TiO₂ composite film. *Ceram. Int.* **2016**, *42*, 2170–2179. [[CrossRef](#)]
15. Gao, L.; Li, J. Preparation of wood-based silver-titanium composite films and its degradation of formaldehyde by visible light. *Sci. Technol. Rev.* **2016**, *34*, 129–133. [[CrossRef](#)]
16. Mishra, S.; Chakinala, N.; Chakinala, A.G.; Surolia, P.K. Photocatalytic degradation of methylene blue using monometallic and bimetallic Bi-Fe doped TiO₂. *Catal. Commun.* **2022**, *171*, 106518. [[CrossRef](#)]
17. Li, J.-Q.; Zhou, Z.-W.; Li, X.; Yang, Y.-L.; Gao, J.-F.; Yu, R.; Wang, H.-P.; Wang, N. Synergistically boosting sulfamerazine degradation via activation of peroxydisulfate by photocatalysis of Bi₂O₃-TiO₂/PAC under visible light irradiation. *Chem. Eng. J.* **2022**, *428*, 132613. [[CrossRef](#)]
18. Xiang, H.; Tuo, B.; Tian, J.; Hu, K.; Wang, J.; Cheng, J.; Tang, Y. Preparation and photocatalytic properties of Bi-doped TiO₂ montmorillonite composite. *Opt. Mater.* **2021**, *116*, 111137. [[CrossRef](#)]
19. Tian, Q.; Li, P.; Cao, P.; Yu, Q. Preparation and Photocatalytic Performance of Bi and Co Doped TiO₂ Ceramic Films. *Bull. Chin. Ceram. Soc.* **2021**, *40*, 3750–3755. [[CrossRef](#)]
20. Kalnaowakul, P.; Phairatana, T.; Ubolchollakhet, K.; Sangchay, W.; Rodchanarowan, A. Synthesis of Bi₂O₃-doped and TiO₂-doped porous Lava for photocatalytic studies. *Mater. Today Proc.* **2018**, *5*, 9312–9318. [[CrossRef](#)]
21. Wang, J.; Pu, W.; Ma, J.; Wang, T.; Zhang, S.; Han, S.; Liu, Z.; Yang, D. Analysis of Band Gap of Inorganic Ruddlesden-Popper Perovskite by Ultraviolet-Visible Diffuse Reflectance Spectroscopy and Tauc Plot Method. *Univ. Phys. Expt.* **2022**, *35*, 13–16. [[CrossRef](#)]
22. Turchi, C.S.; Ollis, D.F. Photocatalytic degradation of organic water contaminants: Mechanisms involving hydroxy radical attack. *J. Catal.* **1991**, *122*, 55–61. [[CrossRef](#)]
23. Fu, X.; Clark, L.A.; Yang, A.Q.; Anderson, M.A. Enhanced photocatalytic performance of titania-based binary metal oxides: TiO₂/SiO₂ and TiO₂/ZrO₂. *Environ. Sci. Technol.* **1996**, *30*, 647–653. [[CrossRef](#)]

24. Rahmani, E.; Ahmadpour, A.; Zebarjad, M. Enhancing the photocatalytic activity of TiO₂ nanocrystalline thin film by doping with SiO₂. *Chem. Eng. J.* **2011**, *174*, 709–713. [[CrossRef](#)]
25. Hu, M.; Lv, C.; Zhao, L.; Wang, X.; Song, Y.; Heng, L. Study on the catalytic luminescence performance of Bi₂O₃-TiO₂ heterojunction nanofibers on toluene. *Chin. J. Anal. Chem.* **2022**, *50*, 1103–1111. [[CrossRef](#)]
26. Ma, X.; Tang, X.; Jin, F.; Shen, B.; Guo, S. Research advancements in the use of TiO₂-based materials for the photocatalytic degradation of volatile organic compounds. *Chin. J. Eng.* **2022**. [[CrossRef](#)]
27. Guo, T.; Yin, Y.; Yu, M. Preparation of Bi-doped TiO₂ nanoparticles based on TiO₂ and its visible light photocatalytic performance. *Energy Sav. Nonferrous Metall.* **2022**, *38*, 37–42. [[CrossRef](#)]
28. Xin, Y.; Wang, X. Effects of codoped Bi and S on the textural properties and photocatalytic activity of TiO₂ nanoparticles. *Chem. Ind. Eng.* **2014**, *31*, 6–12. [[CrossRef](#)]
29. Sun, W.; Liu, Y.; Zhao, Y. Study on preparation and photocatalytic performance of Bi₂O₃-TiO₂. *Anhui Agri. Sci. Bull.* **2016**, *22*, 32–34.
30. Weidong, H.; Wei, Q.; Xiaohong, W.; Hailong, N. Thin bismuth oxide films prepared through the sol–gel method. *Mater. Lett.* **2008**, *61*, 4100–4102. [[CrossRef](#)]
31. Tuerdi, A.; Chen, P.; Abdukayum, A.; Tuerhong, M. Preparation and photocatalytic kinetic of Bismuth doped mesoporous titanium dioxide. *Chin. J. Appl. Chem.* **2016**, *33*, 213–220. [[CrossRef](#)]

Disclaimer/Publisher’s Note: The statements, opinions and data contained in all publications are solely those of the individual author(s) and contributor(s) and not of MDPI and/or the editor(s). MDPI and/or the editor(s) disclaim responsibility for any injury to people or property resulting from any ideas, methods, instructions or products referred to in the content.